A New Method for Designing Modified Compact Microstrip LPF with Sharp Roll-Off and Wide Stopband

Abbas HOSEINABADI [1], Mohammad Bagher TAVAKOLI [2], Mohammad Jalal RASTEGAR FATEMI [1], Farbod SETOUDEH [3]

[1] Dept. of Electronics, Coll. of Engineering, Saveh Branch, Islamic Azad University, Saveh, Iran
[2] Dept. of Electronics, Coll. of Engineering, Arak Branch, Islamic Azad University, Arak, Iran
[3] Dept. of Electrical Engineering, Arak University of Technology, Arak, Iran

{a-hosseinabadi, m-tavakoli}@iau-arak.ac.ir, j_rastegar@iau-saveh.ac.ir, f.setoudeh@arakut.ac.ir

Submitted June 3, 2021 / Accepted October 24, 2021

Abstract. *A new method for designing a compact microstrip lowpass filter (LPF) with wide stopband width (SBW) and sharp roll off (ROF) is presented. In the proposed designing procedure, high impedance microstrip lines are bent to achieve an LPF with compact size. Then, to compensate for the effect of bending microstrip lines, the lengths of the lines are mathematically modified. Moreover, adding a suppressing cell composed of a radial stub resonator and a butterfly stub resonator increases the SBW. Also, an elliptic filter structure is used to obtain sharp ROF. In this work, an LPF with 1.12 GHz cutoff frequency, 0.147 $\lambda_g \times 0.133\ \lambda_g$ filter size; where λ_g is the guided wavelength at cutoff frequency, the SBW equal to 13.4 GHz, and the ROF more than 201 dB / GHz, is designed, simulated and fabricated to demonstrate efficiency of the proposed method. Also, the other conventional characteristics for the fabricated LPF such as 0.3 dB insertion loss, 14.4 dB return loss, and suppression factor equal to 2.2, are in the appropriate range of their amounts.*

Keywords

Lowpass filter, microstrip, elliptic filter, stopband width, roll off, compact size

1. Introduction

In recent decades, the communication systems, especially the microwave applications, benefited from the microstrip filters. The lowpass filters (LPFs) are widely used in most of the communication systems to reject unwanted high frequency signals from system answers [1], [2]. Newly, researchers tried to improve microstrip LPF characteristics such as increasing relative stopband bandwidth (RSB), sharpening roll off (ROF), compacting LPF normalized circuit size (NCS), obtaining low insertion loss (IL) and high return loss (RL) in the passband region, and enhancing suppression factor (SF) in the stopband zone; whereas the ROF, the NCS and the RSB were more considered [3–21]. It should be noted that the RSB, NCS, ROF and SF parameters are commonly used for the LPF and are defined in article [3]. To obtain the high ROF in an LPF that is proposed in [4], stepped impedance modified T-type with stepped impedance stub is used, but it does not have high RSB and the IL is not in the appropriate range. In [5] an LPF using T-shaped resonators is presented to achieve a sharp transition skirt; however its RSB is very small. In [6], the proposed LPF is comprised of three coupled stepped impedance resonators to create the high ROF, while one of disadvantages of this work is the low SF. In some of the reviewed articles, the NCS is more considered. In [7], a folded three-element LPF is proposed to achieve compact size, but its ROF is very low. In other two works [8], [9] the feeding lines are folded to reduce filter size, nevertheless in [9] the RSB is not high and in [8] the ROF is middle and the RSB is also low. Considering the importance of the RSB in the LPF many of the recent papers try to improve the RSB [10–18]. In [10–12] by using stepped impedance resonators the LPFs are designed, and although those have good RSB, their ROFs are very low. In another article [13], the LPF structure is composed of a defected rectangular-shaped resonator and a rectangular shape resonator as a suppressing cell, and amount of its RSB is high, also its NCS is low, nevertheless its ROF is not appropriate. An LPF with wide stopband and low NCS using triangular-shaped resonator is presented in [14], but its ROF is low. Other structures which are used for LPF designing include defected ground structure (DGS) to improve the RSB [15–18]. It is true that using the DGS improves the stopband width, but it complicates filter designing. Also the LPFs that are presented in [15–18] have not high ROF. In another effort an LPF with ultra-wide stopband is proposed [19], while its ROF is moderate and its IL is not acceptable and it also has a complex design. In article [20], using a meandered semi-hairpin resonator which is combined with a suppressing unit, an LPF with wide stopband and small NCS is presented and the disadvantages of it are small ROF and complexity in filter design. In [3], an LPF with good ROF and RSB consisting of two resonators with different triangular patches and four

high-low impedance resonators as suppressing cells has been designed. Finally, in [21], another LPF with good ROF and RSB consisting of three cascaded resonators with different semi-circle patches and four suppressors employing radial stubs has been proposed. But in the last two filters, the NCS is relatively large and those have complex design, too.

In this paper, the use of an elliptic filter structure causes a high ROF. To achieve miniature filter size, the high impedance microstrip lines are bent and their lengths are modified by mathematical analysis. Then as a result of adding suppressing cell, which it consists of a combination of a radial stub resonator and a butterfly stub resonator, the RSB increases. At last, to show efficiency of the designed LPF, it was fabricated and measured.

2. LPF Design Process

2.1 Conventional Elliptic LPF Design

Due to the desired characteristics of an elliptic filter such as high ROF, high SF, and low IL, a six-pole elliptic LPF with 0.1 dB passband ripples and 1.1 GHz cutoff frequency is introduced. Figure 1a shows the LPF prototype circuit with lumped elements. In Fig. 1b layout of the six-pole microstrip LPF is depicted. All inductors and capacitors are realized using high-impedance and low-impedance lines respectively. Characteristic impedance for high-impedance lines $Z_{0L} = 131\ \Omega$, and characteristic impedance for low-impedance lines $Z_{0C} = 20\ \Omega$ are selected. In addition, to calculate high-impedance line lengths l_{Li} for $i = 1,2,\ldots,5$ and low-impedance line lengths l_{Cj} for $j = 2,4,6$, substituting the corresponding parameters from Tab. 1 in (1) is used [2]:

$$l_{Li} = \frac{\lambda_{gL}}{2\pi}\sin^{-1}\left(\frac{2\pi f_c L_i}{Z_{0L}}\right),$$
$$l_{Cj} = \frac{\lambda_{gC}}{2\pi}\sin^{-1}\left(2\pi f_c Z_{0C} C_j\right) \tag{1}$$

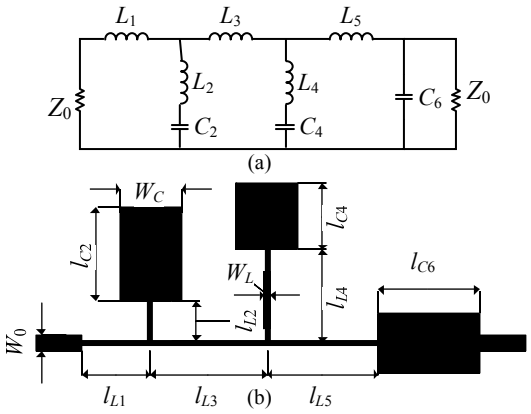

Fig. 1. The conventional elliptic LPF: (a) The prototype circuit with lumped elements. (b) Layout.

Sym.	Value	Sym.	Value	Sym.	Value	Sym.	Value
L_1	4.7378	L_2	3.3256	L_3	7.9020	L_4	6.7163
L_5	7.5280	C_2	2.9041	C_4	2.2371	C_6	2.9557
l_{L1}	7.2	l_{L2}	5	l_{L3}	12.2	l_{L4}	10.3
l_{L5}	11.6	l_{C2}	10.5	l_{C4}	8	l_{C6}	10.7
W_0	1.86	W_L	0.2	W_C	6.5	Z_0	50
λ_{gL}	178.4	λ_{gC}	158.4	f_{p1}	1.298	f_{p2}	1.619

Tab. 1. The values of inductors [nH], capacitors [pF], I/O characteristic impedance [Ω], poles frequency [GHz], wavelengths [mm], widths [mm] and lengths [mm] related to Fig. 1.

where $f_c = 1.1$ GHz is the desired cutoff frequency and λ_{gL} and λ_{gC} are guided wavelengths for high-impedance and low-impedance lines at f_c respectively.

For the LPF with lumped elements two finite-frequency attenuation poles occur at f_{p1} and f_{p2} that are presented by (2). The values of f_{p1} and f_{p2} are also given in Tab. 1 along with other related values in Fig. 1.

$$f_{p1} = \frac{1}{2\pi\sqrt{L_4 C_4}},$$
$$f_{p2} = \frac{1}{2\pi\sqrt{L_2 C_2}}. \tag{2}$$

The compensating for the effect of connecting inductor L_2 to capacitor C_2 which is a discontinuity with different widths, the simultaneous compensation for the unwanted susceptance at the junction of the inductive lines for L_1, L_2, and L_3, is achieved by correcting l_{L2} and l_{C2}, while l_{L1} and l_{L3} are kept unchanged. For this purpose, equation (3) is solved by substituting the cutoff frequency f_c and the attenuation pole frequency f_{p2} instead of f [2]:

$$\frac{1}{2\pi f L_2 - (2\pi f C_2)^{-1}} = B_{b2}(f) + B_T(f) \tag{3}$$

where according to Fig. 1b, $B_{b2}(f)$ specifies the susceptance of L_2 and C_2 branch which was implemented by microstrip lines and will be obtained by (4):

$$B_{b2}(f) = \frac{1}{X_{L2}(f) - \dfrac{1}{B_{C2}(f)}}, \tag{4}$$

$$X_{L2}(f) = Z_{0L}\sin\left(\frac{2\pi l_{L2}}{\lambda_{gL}(f)}\right) + Z_{0C}\tan\left(\frac{\pi l_{C2}}{\lambda_{gC}(f)}\right), \tag{5}$$

$$B_{C2}(f) = \frac{1}{Z_{0C}}\sin\left(\frac{2\pi l_{C2}}{\lambda_{gC}(f)}\right) + \frac{1}{Z_{0L}}\tan\left(\frac{\pi l_{L2}}{\lambda_{gL}(f)}\right). \tag{6}$$

Note that the second term on the right in (5) shows the effect of low impedance line in the step connection related to L_2 and C_2 branch. Similarly, the second term on the right in (6) shows the effect of high impedance line in the step connection related to L_2 and C_2 branch. In (3) $B_T(f)$ is unwanted susceptance resulting T-junction between three high impedance lines l_{L1}, l_{L2} and l_{L3} and it can be written as (7):

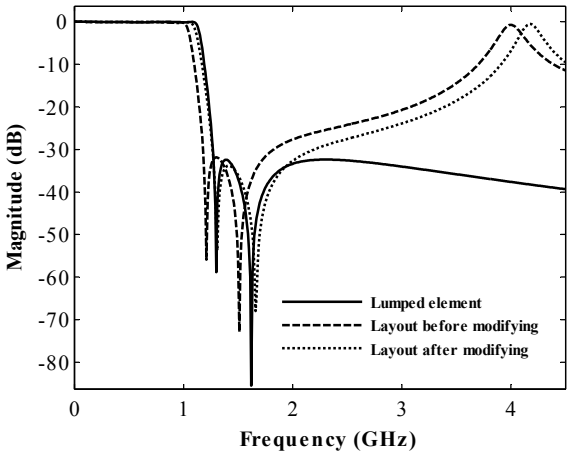

Fig. 2. The simulated S_{21} parameters for the LPF with lumped elements and for the LPF with microstrip layout before and after correcting by (3).

$$B_{\mathrm{T}}(f)=\frac{1}{Z_{0\mathrm{L}}}\tan\left(\frac{\pi l_{\mathrm{L1}}}{\lambda_{\mathrm{gL}}(f)}\right)+\frac{1}{Z_{0\mathrm{L}}}\tan\left(\frac{\pi l_{\mathrm{L2}}}{\lambda_{\mathrm{gL}}(f)}\right)+\frac{1}{Z_{0\mathrm{L}}}\tan\left(\frac{\pi l_{\mathrm{L3}}}{\lambda_{\mathrm{gL}}(f)}\right). \quad (7)$$

Also for L_4 and C_4 branch an equation similar to (3) should be written by replacing the parameters corresponding to it then solved at f_c and f_{p1}. After correcting, the lengths of the corrected lines are obtained as $l_{L2} = 4$ mm, $l_{C2} = 10.7$ mm, $l_{L4} = 9.2$ mm and $l_{C4} = 7.7$ mm. In Fig. 2 S_{21} parameter responses for the LPF with lumped elements and microstrip layout before and after correcting by (3) are illustrated. As shown in Fig. 2 locations of f_{p1} and f_{p2} in the LPF with microstrip layout after correcting by (3) and the LPF with lumped elements are almost matched.

2.2 Compacting LPF Size

The dimensions of the filter can be reduced by using the technique of bending high impedance microstrip lines. Of course, it should be noted that bending the microstrip lines causes unwanted effects on the values of inductors and capacitors implemented with microstrip lines. To correct the deviation in the inductor and the capacitor values, which means deviation in electrical length of microstrip lines, the physical length of the lines must be modified. For example, Figure 3 shows how l_{L2} and l_{L3} are bent to reduce the filter size.

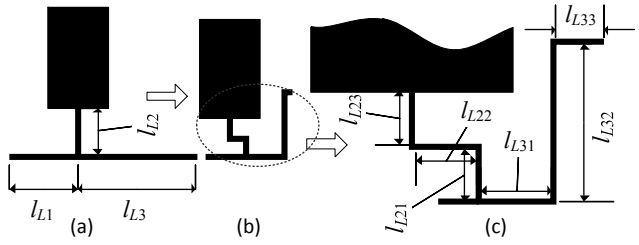

Fig. 3. Bending microstrip lines to reduce filter size: (a) Before bending, (b) after bending, (c) detailed.

To modify the deviation caused by bending of l_{L2} and l_{L3}, susceptance $B_{2\mathrm{Bent}}(f)$ that is presented in (8) is added to the right side of (3). Then (3) can be rewritten in form of (9):

$$B_{2\mathrm{Bent}}=\frac{1}{Z_{0\mathrm{L}}}\left(\tan\left(\frac{\pi l_{\mathrm{L21}}}{\lambda_{\mathrm{gL}}(f)}\right)+2\tan\left(\frac{\pi l_{\mathrm{L22}}}{\lambda_{\mathrm{gL}}(f)}\right)+\tan\left(\frac{\pi l_{\mathrm{L23}}}{\lambda_{\mathrm{gL}}(f)}\right)+\tan\left(\frac{\pi l_{\mathrm{L31}}}{\lambda_{\mathrm{gL}}(f)}\right)+2\tan\left(\frac{\pi l_{\mathrm{L32}}}{\lambda_{\mathrm{gL}}(f)}\right)+\tan\left(\frac{\pi l_{\mathrm{L33}}}{\lambda_{\mathrm{gL}}(f)}\right)\right), \quad (8)$$

$$\frac{1}{2\pi fL_2-(2\pi fC_2)^{-1}}=B_{\mathrm{b2}}(f)+B_{\mathrm{T}}(f)+B_{2\mathrm{Bent}}(f). \quad (9)$$

The values of $l_{L31} = 3.2$ mm, $l_{L32} = 8.1$ mm and $l_{L33} = 0.9$ mm are considered but the values of $l_{L21} = 1.3$ mm, $l_{L22} = 1.2$ mm and $l_{L23} = 1.5$ mm are first estimated. After solving by substituting the cutoff frequency f_c and the attenuation pole frequency f_{p2} instead of f in (9) new values for $l_{L2} = 3.5$ mm and $l_{C2} = 11.7$ mm are obtained. After determining new values for l_{L2} and l_{C2}, new values $l_{L21} = 1.1$ mm, $l_{L22} = 1$ mm and $l_{L23} = 1.4$ mm can be selected accordingly. Correction the lengths of l_{L4} and l_{C4} are similar to the method described in this section and could be done by replacing the parameters proportional to the L_4C_4 branch. After the correction process of the L_4C_4 branch, values of $l_{L4} = 8.5$ mm and $l_{C4} = 8.3$ mm are obtained.

Figure 4 illustrates EM simulated S_{21} parameters for modified bended layout by (9) for L_2C_2 branch which is shown in Fig. 3b (and L_4C_4 branch but not shown), beside S_{21} parameters for the lumped elements circuit corresponding to connection of L_1, L_2, L_3 and C_2 (or L_3, L_4, L_5 and C_4 for L_4C_4 branch). Also, Figure 4 shows EM simulated S_{21} parameters for unmodified bended layout of L_2C_2 and L_4C_4

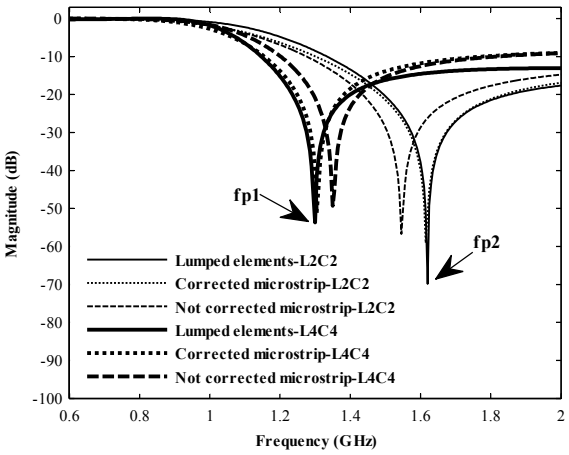

Fig. 4. The S_{21} parameters of the L_2C_2 or L_4C_4 branches: solid line (or bold solid line) for L_2C_2 (or L_4C_4) branch with lumped elements, dot line (or bold dot line) for L_2C_2 (or L_4C_4) branch with microstrip lines which bended then corrected with (9), and finally dash line (or bold dash line) for L_2C_2 (or L_4C_4) branch with microstrip lines which bended but not corrected with (9).

branches for comparing. As shown in Fig. 4 the location of f_{p1} and f_{p2} deviate by bending microstrip high impedance lines from values predicted with (2) however, the correction of the microstrip line lengths by (9) can match the values of f_{p1} and f_{p2} to values which obtained by (2). The S_{21} parameters for the corrected bended microstrip layouts and the lumped element circuits are well matched. This match causes the modified LPF cutoff frequency closes to cutoff frequency of the LPF with lumped elements.

2.3 Adding Suppression Resonators

It can be seen by looking at Fig. 2 that the microstrip conventional elliptic LPF has a narrow SBW. In order to increase the SBW, a suppression cell consisting of two resonators has been used. Generating transmission zeros (TZs) at frequencies higher than the cutoff frequency can increase the SBW but this action should not interfere with the filter frequency response at frequencies below the cutoff frequency. As shown in Fig. 5, a combination of a radial stub resonator (RSR) and a butterfly stub resonator (BSR) in the middle of l_{L5} forms a suppression cell. Now l_{L5} is no longer valid and is replaced by l_{L5-1}, l_{L5-2} and l_{L5-3}. The lengths of l_{L5-1}, l_{L5-2} and l_{L5-3} are selected by using ADS software tuning application. The values l_{L5-1} = 6.5 mm, l_{L5-2} = 6.4 mm and l_{L5-3} = 6.1 mm is obtained. The RSR structure is shown in Fig. 6. The values of parameters corresponding to Fig. 6a are R_{RS} = 7.4 mm, r_{RS} = 0.58 mm, θ_{RS} = 120°. The equivalent lossless circuit with lumped elements is illustrated in Fig. 6b [22]. Assuming $R_{RS} < \lambda_g/8$ and $r_{RS} \approx R_{RS}/10$, the values of C_{RS} and L_{RS} are extracted from (10) and (11) [23]:

$$C_{RS} = \frac{\theta_{RS} R_{RS}^2 \varepsilon_{eff}}{240\pi hc}, \tag{10}$$

$$L_{RS} = \frac{120\pi h\left(2.8 - 10 r_{RS}/R_{RS}\right)}{c\theta_{RS}} \tag{11}$$

where ε_{eff} is effective dielectric constant of microstrip line with width equal to $w_{eq} = (R_{RS} + r_{RS}) \sin(\theta_{RS}/2)$, also h = 0.813 mm is dielectric thickness and c is speed of light. As a result, the transmission zero for the RSR (TZ1) can be written as follows:

$$f_{TZ1} = \frac{1}{2\pi\sqrt{L_{RS} C_{RS}}}. \tag{12}$$

A T-junction is used to connect the RSR to the high impedance microstrip line. Adding the T-junction causes the TZ1 position deviates from the value obtained by (12). To correct adding T-junction effect the LC equivalent circuit of T-junction is appended to the LC equivalent circuit of the RSR. The appending of the LC equivalent circuit of the RSR and the LC equivalent circuit of the T-junction are shown in Fig. 6d.

The values for T-junction are w_{1T} = 0.2 mm and w_{2T} = 1 mm. The values of C_T [pF], L_{1T} and L_{2T} are extracted from (13), (14) and (15) with (16) [24], [25]:

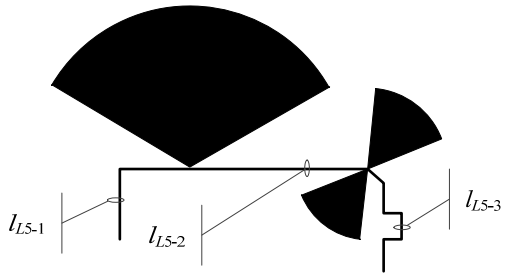

Fig. 5. The RSR and the BSR located at middle of l_{L5}.

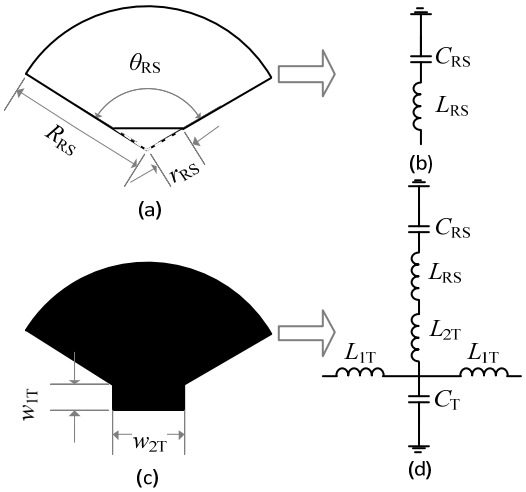

Fig. 6. The RSR structure and its LC model: (a) The RSR schematic. (b) The LC equivalent circuit of the RSR. (c) The RSR with T-junction schematic. (d) The LC equivalent circuit of the T-junction is appended to the LC equivalent circuit of the RSR.

$$\frac{C_T}{w_{1T}} = \frac{100}{\tanh\left(0.0072 Z_0\right)} + 0.64 Z_0 - 261.0, \tag{13}$$

$$\frac{L_{1T}}{h} = \frac{-w_{2T}}{h}\left[\frac{w_{2T}}{h}\left(-0.016\frac{w_{1T}}{h} + 0.064\right) + \frac{0.016h}{w_{1T}}\right] L_{w,1}, \tag{14}$$

$$\frac{L_{2T}}{h} = \left[\left(\frac{0.12 w_{1T}}{h} - 0.47\right)\frac{w_{2T}}{h} + 0.195\frac{w_{1T}}{h} - 0.357 + 0.0283\sin\left(\frac{\pi w_{1T}}{h} - 0.75\pi\right)\right] L_{w,2}, \tag{15}$$

$$L_{w,n} = \frac{Z\left(w_{nT}\right)\sqrt{\varepsilon_{eff}\left(w_{nT}\right)}}{c}\,[\text{nH}] \tag{16}$$

where $Z(w_{nT})$ and ε_{eff} (w_{nT}) are characteristic impedance and effective dielectric constant of w_{nT} (w_{1T} or w_{2T}) respectively.

The values of capacitors and inductors which related to Fig. 6 are brought in Tab. 2. Now the transmission zero for the RSR can be rewritten as follows:

$$f_{TZ1} = \frac{1}{2\pi\sqrt{\left(L_{RS} + L_{1T}\right) C_{RS}}}. \tag{17}$$

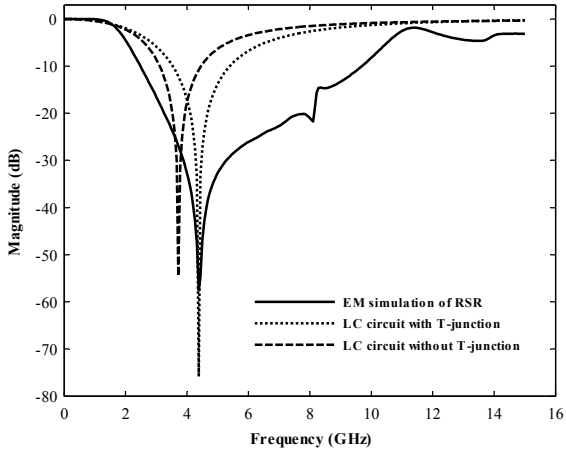

Fig. 7. The solid line shows the S_{21} parameters of the microstrip RSR which is simulated EM; also the dot line and dash line show the S_{21} parameters of LC equivalent circuit of the RSR with and without T-junction LC equivalent circuit respectively.

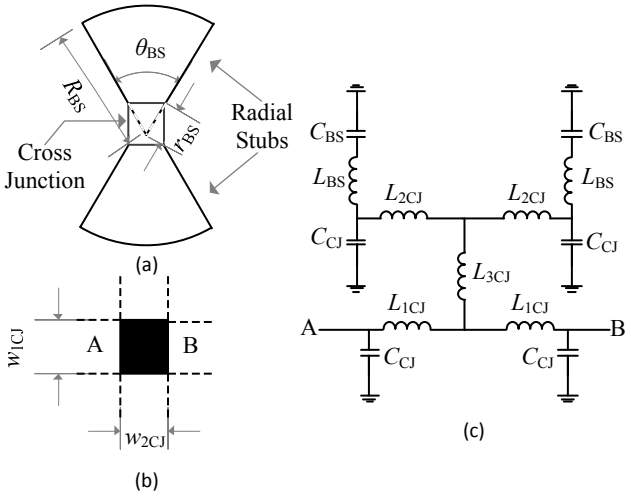

Fig. 8. The BSR structure and its LC model: (a) The BSR schematic which is created by combining two RSR with one cross junction. (b) The cross junction schematic. (c) The LC equivalent circuit of the BSR.

And f_{TZ1} is obtained from (17) with value 4.3 GHz. As shown in Fig. 7 the TZ1 in both the S_{21} parameter curves of the RSR resonator with T-junction and its LC equivalent circuit is matched. In Fig. 8 the BSR structure is depicted. As shown in Fig. 8a the BSR structure is created by combining two RSR with one cross junction. Also the LC equivalent circuit of the BSR is depicted in Fig. 8c. The values of the BSR are $R_{BS} = 4$ mm, $r_{BS} = 0.47$ mm, $\theta_{BS} = 65°$. The values of cross junction are $w_{1CJ} = 0.2$ mm and $w_{2CJ} = 0.51$ mm. The value of the parameters of C_{BS} and L_{BS} are extracted from (10) and (11) by substituting the RSR parameters with the related BSR parameters. In addition, the calculation of parameters C_{CJ}, L_{1CJ}, L_{2CJ} and L_{3CJ} is performed using (A1), (A2), (A3) and (A4) [24], [25] which are given in Appendix A. Also, the values of C_{CJ}, L_{1CJ}, L_{2CJ} and L_{3CJ} are brought in Tab. 2. In next, ignoring the parameter C_{CJ}, the transmission zero of the BSR (TZ2) can be written as:

Sym.	Value	Sym.	Value	Sym.	Value	Sym.	Value
L_{RS}	0.9833	C_{RS}	1.858	L_{1T}	–0.0934	L_{2T}	–0.2724
C_T	–0.0012	L_{BS}	1.454	C_{BS}	0.2685	L_{1CJ}	0.0894
L_{2CJ}	0.0490	L_{3CJ}	–0.3135	C_{CJ}	–0.0681	ε	3.38

Tab. 2. The values of inductors [nH] and capacitors [pF] related to Fig. 6 and Fig. 8.

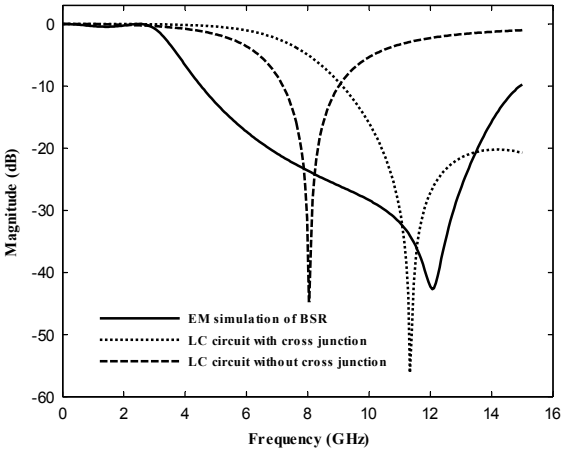

Fig. 9. The solid line shows the S_{21} parameters of the microstrip BSR which is simulated EM; also the dot line and dash line show the S_{21} parameters of LC equivalent circuit of the RSR with and without cross junction LC equivalent circuit respectively.

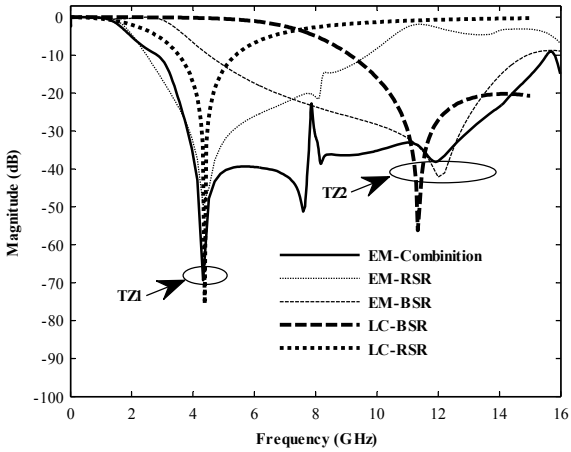

Fig. 10. The S_{21} parameters of the RSR, the BSR and the combination of them which are EM simulated, and the S_{21} parameters of LC equivalent circuit of the RSR and the BSR.

$$f_{TZ2} = \frac{1}{2\pi\sqrt{(L_{BS} + L_{2CJ} + 2L_{3CJ})C_{BS}}}. \qquad (18)$$

The f_{TZ2} is obtained from (18) with value 10.38 GHz. This value is near to the f_{TZ2} which is obtained from EM simulation of the BSR (12 GHz). As shown in Fig. 9 the TZ2 in both the S_{21} parameter curves of the BSR resonator and its LC equivalent circuit is almost matched.

Also, Figure 10 shows the S_{21} parameters of the RSR and the BSR resonators separately, combined and those LC equivalent circuits. As shown in Fig. 10 both resonators and combination of them have low IL in the passband.

These resonators add two transmission zeros at f_{TZ1} = 4.3 GHz and f_{TZ2} = 12 GHz, but due to their appropriate frequency responses at low frequencies do not appear significant change in the S_{21} parameter in the passband region. Also attenuation of better than 20 dB of the suppression cell in the frequency range of 3.5 GHz to 14.4 GHz causes the stop bandwidth to be increased appropriately.

3. Comparing Results of Simulation and Measurement

Figure 11 shows the final design of the proposed LPF. Most of the values of the parameters related to Fig. 11 were determined in the previous sections however, the newly introduced parameters are $l_{L5–11}$ = 3 mm, $l_{L5–12}$ = 3.5 mm, $l_{L5–31}$ = 0.9 mm, $l_{L5–32}$ = 1.5 mm, $l_{L5–33}$ = 1 mm, $l_{L5–34}$ = 0.8 mm, $l_{L5–35}$ = 1.1 mm, l_{L41} = 6.7 mm and l_{L42} = 1.8 mm. The proposed LPF is simulated with the Agilent ADS software. Then the LPF is fabricated on RO4003C substrate with 0.813 mm thickness, dielectric constant (ε_r) equal to 3.38 and loss tangent (δ) equal to 0.0021. The fabricated LPF is measured with the Agilent E8362B network analyzer. The actual photograph of the fabricated LPF is shown in Fig. 12. The results of S_{21} and S_{11} parameters simulation and measurement are illustrated in Fig. 13. Based on measurement results, the cutoff frequency is set at 1.12 GHz. The 20 dB attenuation SBW is obtained 13.4 GHz (from 1.2 to 14.6 GHz) which it causes the RSB to be equal to 1.7 and the ratio of the SBW to cutoff frequency (SBW / f_c) to be equal to 12. However the IL is less than 0.3 dB (0–816 MHz) and the RL is at least 14.4 dB, in addition the SF is 2.2.

For six-pole elliptic LPF with lumped elements which is shown in Fig. 1a the ROF from 3 dB to 40 dB is a maximum of about 269 dB / GHz. For the proposed LPF a good ROF more than 201 dB / GHz is obtained which means 75% of the LPF with lumped elements. In order to achieve a higher ROF, the degree of filter must be larger, which makes the IL unsuitable in addition to filter complexity. Table 3 compares the important parameters of filter with the results of the recent reviewed research. Note that some of compared articles in Tab. 3 have high ROF [4–6] however, compared to the present work in [4] the IL is not appropriate and in [4], [5] the RSB is very small. Also, in [6] the SF is small and other important parameters are not very appropriate. Using the microstrip line bending method the value of the NCS was reduced from 0.255 $\lambda_g \times 0.125\ \lambda_g$ (for not bended LPF) to 0.147 $\lambda_g \times 0.133\ \lambda_g$, that means 39% reduction. As can be deduced from Tab. 3, the method that presented in this paper works well for increasing the SBW and decreasing the NCS, while high ROF is obtained and the other LPF important parameters are in the proper range. It is necessary to mention that ROF (ζ), SF, RSB and NCS parameters for the LPF are very common and widely used parameters. The ROF is defined as:

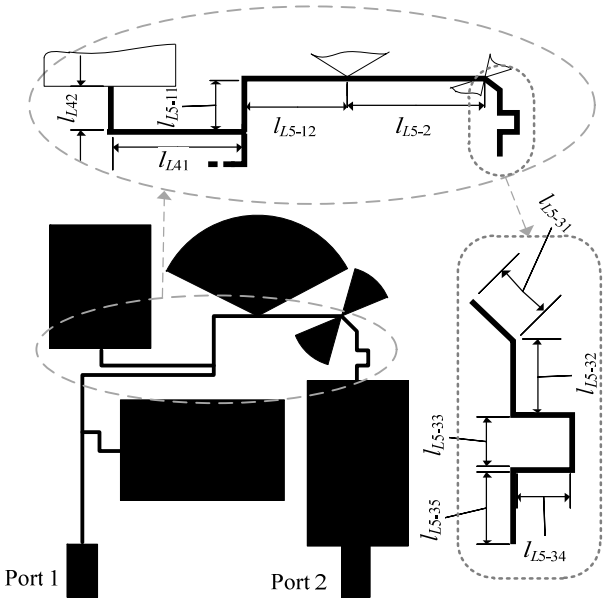

Fig. 11. The layout of final proposed LPF along its remaining details.

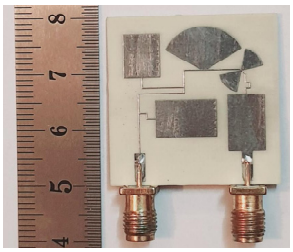

Fig. 12. The actual photograph of the fabricated LPF.

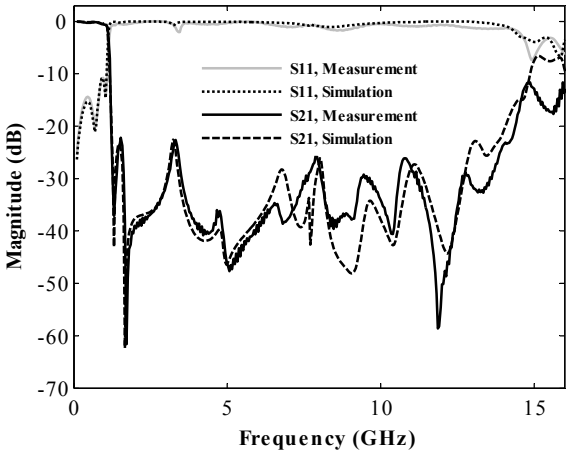

Fig. 13. Comparing the simulated and measured S-parameters for the proposed LPF.

$$\zeta = \frac{\alpha_{max} - \alpha_{min}}{f_s - f_c} \tag{19}$$

where in this paper α_{max} = 40 dB, α_{min} = 3 dB and f_s is the first frequency whose attenuation is 40 dB. The SF, the RSB and the NCS are given by (20), (21) and (22) respectively:

Ref.	f_c	ζ	IL	RL	SF	RSB	NCS
[3]	1.8	228	-	17.3	2.1	1.78	0.229 × 0.140
[4]	1.24	336	0.88	14	1.93	1.33	0.100 × 0.150
[5]	1.32	411	-	17	2.8	1.00	0.158 × 0.128
[6]	1.95	440	0.4	12	1.5	1.56**	0.271 × 0.122
[7]	1.64	57.8	-	-	3.5	1.61	0.120 × 0.100
[8]	3.8	87.3	0.1	21	2.8	1.09**	0.138 × 0.158
[9]	2.68	-	0.12	18.5	2	1.51**	(147.6)
[10]	2.8	48.5	0.1	16.5	2	1.61	0.141 × 0.151
[11]	0.9	81*	0.5	15.5	2.24**	1.78**	0.176 × 0.102
[12]	2.92	35.4	0.12	16	2	1.65**	0.156 × 0.128
[13]	1.44	90.2	0.2	14	2	1.65	(132)
[14]	1.52	90	0.2	17	2	1.66	0.062 × 0.104
[15]	1.2	135	0.35	20.6	2	1.71	0.237 × 0.105
[16]	2	41	0.3	-	2	1.64	0.140 × 0.100
[17]	2.49	37.2	0.8	7.6	1.5	1.62	0.180 × 0.210
[18]	4.2	6.14	0.5	-	1**	0.749	0.417 × 0.202
[19]	1.96	104	0.6	12	2.5	1.8	0.189 × 0.121
[20]	2.2	63**	0.2	17.4	2	1.73	0.113 × 0.107
[21]	2.1	203	0.1	-	3.2	1.61	0.208 × 0.208
This work	1.12	201	0.3	14.4	2.2	1.7	0.147 × 0.133

*- for 60 dB attenuation

**- calculated with the information given in the related article

Tab. 3. Comparison of f_c [GHz], ζ [dB/GHz], IL [dB], RL [dB], SF, RSB and NCS [$\lambda_g \times \lambda_g$] or (mm^2) parameters between the proposed LPF in this work and the reviewed recent articles.

$$\mathrm{SF} = \frac{\text{rejection level}\,[\mathrm{dB}]}{10\,[\mathrm{dB}]}, \tag{20}$$

$$\mathrm{RSB} = \frac{\text{stopband bandwidth}}{\text{stopband center frequency}}, \tag{21}$$

$$\mathrm{NCS} = \frac{\text{physical size (length} \times \text{width)}}{\lambda_g^2}. \tag{22}$$

4. Conclusion

In this paper by using the microstrip lines bending technique the LPF size reduced 39%. In order to match S_{21} responses between the bended LPF and the lumped elements circuit, the microstrip line lengths were modified mathematically. Adding surplus suppression resonators led to increase the SBW up to 12 times the cutoff frequency. Taking the advantage of the elliptic structure for the LPF caused a high ROF up to 201 dB / GHz. Low IL, high RL, high SF, simple architecture and low cost are other benefits of the proposed LPF. Finally, close matching results between simulation and measurement represents advantages of using the method proposed in this article.

References

[1] POZAR, D. M. *Microwave Engineering*. 2nd ed. New York (USA): John Wiley & Sons, Inc., 1998. ISBN: 9780471170969

[2] HONG, J.-S., LANCASTER, M. J. *Microstrip Filters for RF/Microwave Applications*. New York (USA): John Wiley & Sons, Inc., 2001. DOI: 10.1002/0471221619

[3] ABDIPOUR, AS., ABDIPOUR, AR., KOSRAVI, A. A compact microstrip lowpass filter with ultra-wide rejection band and sharp transition band utilizing combined resonators with triangular patches. *Radioengineering,* 2018, vol. 27, no. 2, p. 417–424. DOI: 10.13164/re.2018.0417

[4] PHANI KUMAR, K. V., KARTHIKEYAN, S. S. Microstrip lowpass filter with flexible roll-off rates. *AEU International Journal of Electronics and Communications,* 2018, vol. 86, p. 63–68. DOI: 10.1016/j.aeue.2018.01.025

[5] ROSHANI, S., GOLESTANIFAR, A., GHADERI, A., et al. High performance microstrip low pass filter for wireless communications. *Wireless Personal Communications,* 2017, vol. 99, no. 1, p. 497–507. DOI: 10.1007/s11277-017-5123-1

[6] KUMAR, L., PARIHAR, M. S. A wide stopband low-pass filter with high roll-off using stepped impedance resonators. *IEEE Microwave and Wireless Components Letters,* 2018, vol. 28, no. 5, p. 404–406. DOI: 10.1109/lmwc.2018.2816520

[7] ZHANG, B., LI, S., HUANG, J. Compact lowpass filter with wide stopband using coupled rhombic stubs. *Electronics Letters,* 2015, vol. 51, no. 3, p. 264–266. DOI: 10.1049/e1.2014.3490

[8] RAMANUAJAM, P., RAMESH VENKATESAN, P. G., ARUMUGAM, C. Miniaturized low-pass filter design with wide stopband using complementary split-ring resonator. *Microwave and Optical Technology Letters,* 2019, vol. 61, no. 12, p. 2832–2837. DOI: 10.1002/mop.31951

[9] SHEIKHI, A., ALIPOUR, A., ABDIPOUR, A. Design of compact wide stopband microstrip low-pass filter using T-shaped resonator. *IEEE Microwave and Wireless Components Letters,* 2017, vol. 27, no. 2, p. 111–113. DOI: 10.1109/lmwc.2017.2652862

[10] SHEIKHI, A., ALIPOUR, A., HEMESI, H. Design of microstrip wide stopband lowpass filter with lumped equivalent circuit. *Electronics Letters,* 2017, vol. 53, no. 21, p. 1416–1418. DOI: 10.1049/el.2017.1715

[11] CHEN, F. C., LI, R. S, CHU, Q. X. Ultra-wide stopband low-pass filter using multiple transmission zeros. *IEEE Access,* 2017, vol. 5, p. 6437–6443. DOI: 10.1109/access.2017.2693344

[12] HAYATI, M., SHAMA, F. A compact lowpass filter with ultra wide stopband using stepped impedance resonator. *Radioengineering,* 2017, vol. 26, no. 1, p. 269–274. DOI: 10.13164/re.2017.0269

[13] EKHTERAEI, M., HAYATI, M., KAZEMI, A. H., et al. Design and analysis of a modified rectangular-shaped lowpass filter based on LC equivalent circuit. *AEU – International Journal of Electronics and Communications,* 2020, vol. 126, p. 1–9. DOI: 10.1016/j.aeue.2020.153290

[14] LOTFI, S., HAYATI, M. Compact low-pass filter with ultra-wide stopband using analysed triangular-shaped resonator. *Electronics Letters,* 2017, vol. 53, no. 15, p. 1050–1052. DOI: 10.1049/el.2017.1169

[15] SEN, S., MOYRA, T. Compact low-cost microstrip lowpass filter with sharp roll-off and wide attenuation band. *International*

Journal of RF and Microwave Computer-Aided Engineering, 2019, vol. 29, no. 11. DOI: 10.1002/mmce.21917

[16] SEN, S., MOYRA, T. A compact lowpass filter using interdigital line resonator with wide stopband. *Iranian Journal of Science and Technology, Transactions of Electrical Engineering,* 2019, vol. 43, no. 3, p. 469–478. DOI: 10.1007/s40998-019-00191-w

[17] SHI, L., FAN, Z., XIN, D. Miniaturized low-pass filter based on defected ground structure and compensated microstrip line. *Microwave and Optical Technology Letters,* 2019, vol. 62, no. 3, p. 1093–1097. DOI: 10.1002/mop.32144

[18] SINGHAL, D., SINGH, S., KAUSHAL, V., et al. Wide band stop response using interdigital capacitor/CSRR DGS in elliptical microstrip low-pass filter. *Journal of Microwaves, Optoelectronics and Electromagnetic Applications,* 2020, vol. 19, no. 4, p. 495–509. DOI: 10.1590/2179-10742020v19i4945

[19] JIANG, S., XU, J. Sharp roll-off planar lowpass filter with ultra-wide stopband up to 40 GHz. *Electronics Letters,* 2017, vol. 53, no. 11, p. 734–735. DOI: 10.1049/el.2017.1238

[20] SHAMA, F., HAYATI, M., EKHTERAEI, M., et al. Compact microstrip lowpass filter using meandered unequal T-shaped resonator with ultra-wide rejection band. *AEU – International Journal of Electronics and Communications,* 2018, vol. 85, p. 78–83. DOI: 10.1016/j.aeue.2017.12.038

[21] ABDIPOUR, AS., ABDIPOUR, AR., ALAHVERDI, M. A design of microstrip lowpass filter with wide rejection band and sharp transition band utilizing semi-circle resonators. *Radioengineering,* 2018, vol. 27, no. 4, p. 1043–1049. DOI: 10.13164/re.2018.1043

[22] GIANNINI, F., PAOLONI, C., RUGGII, M. CAD-oriented lossy models for radial stubs. *IEEE Transactions on Microwave Theory and Techniques,* 1988, vol. 36, no. 2, p. 305–313. DOI: 10.1109/22.3519

[23] KWON, H., LIM, H., KANG, B. Design of 6–18 GHz wideband phase shifters using radial stubs. *IEEE Microwave and Wireless Components Letters,* 2007, vol. 17, no. 3, p. 205–207. DOI: 10.1109/lmwc.2006.890481

[24] WADELL, B. C. *Transmission Line Design Handbook*. Norwood (USA): Artech House, 1991. ISBN: 0890064369

[25] GARG, R., BAHL, I. J. Microstrip discontinuities. *International Journal of Electronics,* 1978, vol. 45, no. 1, p. 81–87. DOI: 10.1080/00207217808900883

About the Authors ...

Abbas HOSEINABADI received his B.Sc. and M.Sc. from Electronics Department of Arak branch, Islamic Azad University. He is currently a Ph.D. student at Electronics Department of Saveh branch, Islamic Azad University.

Mohammad Bagher TAVAKOLI received his Ph.D. in Electronics from Science and Research branch, Islamic Azad University in 2013 and his M.Sc. and B.Sc. from Electronics Department of Arak branch, Islamic Azad University. He is currently an Associate Professor at the Islamic Azad University of Arak and the Dean of the Faculty of Engineering in Islamic Azad University of Arak.

Mohammad Jalal RASTEGAR FATEMI received the M.Sc. degree from Azad University of Arak 2006 and the Ph.D. degree in the Dept. of Electrical Engineering, University of Science and Research of Tehran 2011, both in Electronic Engineering. He joined the Azad University of Saveh in 2006 as lecturer. His research interests focus on power electronics and semiconductor device modeling and he does some researches on image processing and computer vision.

Farbod SETOUDEH received his Ph.D. degree in Electrical Engineering from Science and Research Branch of Azad University and is currently an Assistant Professor at Electrical Engineering Department of Arak University of Technology. His research interests include intelligent system, signal processing, and nonlinear system.

Appendix A: Computational Equations of C_{CJ}, L_{1CJ}, L_{2CJ} and L_{3CJ}

In this appendix, the computational equations for the LC equivalent circuit of cross junction (A1), (A2), (A3) and (A4) are presented. All necessary parameters and the results of calculation have been given in Sec. 2.3.

$$\frac{C_{CJ}}{w_{1CJ}} = \left\{\left[\frac{86.6w_{2CJ}}{h} - 30.9\sqrt{\frac{w_{2CJ}}{h}} + 367.0\right]\log\left(\frac{w_{1CJ}}{h}\right) + \left(\frac{w_{2CJ}}{h}\right)^3 + \frac{74.0w_{2CJ}}{h} + 130.0\right\}\left(\frac{w_{1CJ}}{h}\right)^{-1/3} - 240.0 + \frac{2.0h}{w_{2CJ}} - \frac{1.5w_{1CJ}}{\mathrm{h}}\left(1.0 - \frac{w_{2CJ}}{h}\right), \tag{A1}$$

$$\frac{L_{1CJ}}{h} = \left\{\left[\frac{165.6w_{2CJ}}{h} + 31.2\sqrt{\frac{w_{2CJ}}{h}} - 11.8\left(\frac{w_{2CJ}}{h}\right)^2\right]\frac{w_{1CJ}}{h} - \frac{32.0w_{2CJ}}{h} + 3.0\right\}\left(\frac{w_{1CJ}}{h}\right)^{-3/2}, \tag{A2}$$

$$\frac{L_{2CJ}}{h} = \left\{\left[\frac{165.6w_{1CJ}}{h} + 31.2\sqrt{\frac{w_{1CJ}}{h}} - 11.8\left(\frac{w_{1CJ}}{h}\right)^2\right]\frac{w_{2CJ}}{h} - \frac{32.0w_{1CJ}}{h} + 3.0\right\}\left(\frac{w_{2CJ}}{h}\right)^{-3/2}, \tag{A3}$$

$$\frac{L_{3CJ}}{h} = 337.5 + \left(1 + \frac{7h}{w_{1CJ}}\right)\frac{h}{w_{2CJ}} - \frac{5.0w_{2CJ}}{h}\cos\left[\frac{\pi\left(1.5h - w_{1CJ}\right)}{2h}\right]. \tag{A4}$$